Three-Dimensional Quasi-linear Electromagnetic Modeling and Inversion

Michael S. Zhdanov
Sheng Fang

Summary. The quasi-linear (QL) approximation replaces the (unknown) total field in the integral equation of electromagnetic (EM) scattering with a linear transformation of the primary field. This transformation involves the product of the primary field with a reflectivity tensor, which is assumed to vary slowly inside inhomogeneous regions and therefore can be determined numerically on a coarse grid by a simple optimization. The QL approximation predicts EM responses accurately over a wide range of frequencies for conductivity contrasts of more than 100 to 1 between the scatterer and the background medium. It also provides a fast-forward model for 3-D EM inversion. The inversion equation is linear with respect to a modified material property tensor, which is the product of the reflectivity tensor and the anomalous conductivity. We call the (regularized) solution of this equation a *quasi-Born inversion.* The material property tensor (obtained by inversion of the data) then is used to estimate the reflectivity tensor inside the inhomogeneous region and, in turn, the anomalous conductivity. Solution of the nonlinear inverse problem thus proceeds through a set of linear equations. In practice, we accomplish this inversion through gradient minimization of a cost function that measures the error in the equations and includes a regularization term. We use synthetic experiments with plane-wave and controlled sources to demonstrate the accuracy and speed of the method.

1 Introduction

There has been great progress recently in 3-D electromagnetic (EM) modeling and inversion with both integral-equation (Eaton, 1989; Xiong, 1992; Xiong and Kirsch, 1992; Tripp and Hohmann, 1993; Xiong and Tripp, 1993; Xie and Lee, 1995) and finite-difference methods (Madden and Mackie, 1989; Newman and Alumbaugh, 1995). These "exact" methods, however, usually require too large a computational effort to allow their routine use. We have been developing a practical 3-D inversion based on a fast new method of forward modeling called the quasi-linear (QL) approximation (Zhdanov and Fang, 1996a). In the QL approximation, the anomalous field inside the

Department of Geology and Geophysics, University of Utah, Salt Lake City, UT 84112, USA.

the Born approximation for the scattering (Born, 1933):

$$\mathbf{E}^B(\mathbf{r}_j) = \iiint_D \underset{\sim}{\mathbf{G}}^n(\mathbf{r}_j \mid \mathbf{r})\Delta\tilde{\sigma}(\mathbf{r})\mathbf{E}^n(\mathbf{r})\,dv. \tag{3}$$

This approximation, however, is not very accurate for EM scattering by the large conductivity contrasts (or large bodies) that are typical of geophysical problems. Habashy et al. (1993) and Torres-Verdın and Habashy (1994) developed the extended Born approximation, which replaces the internal field in the integral (2) not by the normal field, but by its projection onto a scattering tensor $\underset{\sim}{\Gamma}(r)$:

$$\mathbf{E}(\mathbf{r}) = \underset{\sim}{\Gamma}(\mathbf{r})\mathbf{E}^n(\mathbf{r}). \tag{4}$$

An expression for the scattering tensor is derived by rewriting Eq. (2) as an integral equation for the total field,

$$\mathbf{E}(\mathbf{r}_j) = \mathbf{E}^n(\mathbf{r}_j) + \iiint_D \underset{\sim}{\mathbf{G}}^n(\mathbf{r}_j \mid \mathbf{r})\Delta\tilde{\sigma}(\mathbf{r})\mathbf{E}(\mathbf{r})\,dv, \tag{5}$$

and then approximating $\mathbf{E}(\mathbf{r})$ in the integral by its value at the point $\mathbf{r}_j$.

$$\mathbf{E}(\mathbf{r}_j) \approx \mathbf{E}^n(\mathbf{r}_j) + \mathbf{E}(\mathbf{r}_j)\iiint_D \underset{\sim}{\mathbf{G}}^n(\mathbf{r}_j \mid \mathbf{r})\Delta\tilde{\sigma}(\mathbf{r})\,dv, \tag{6}$$

or

$$\mathbf{E}(\mathbf{r}_j) \approx \left[\mathbf{I} - \iiint_D \underset{\sim}{\mathbf{G}}^n(\mathbf{r}_j \mid \mathbf{r})\Delta\tilde{\sigma}(\mathbf{r})\,dv\right]^{-1} \mathbf{E}^n(\mathbf{r}_j). \tag{7}$$

The expression in brackets is the scattering tensor; it does not depend on the illuminating sources and is an explicit nonlinear functional of the anomalous conductivity. In forward modeling with the extended Born approximation, the scattering tensor can be calculated directly; in inversion, the scattering tensor is calculated for an (assumed) initial model, and then updated iteratively after solving an inverse problem for the anomalous conductivity. Torres-Verdin and Habashy (1994) also showed that, for some models, the iterative procedure could be collapsed into a simple two-step inversion.

2.2 QL approximation

In Zhdanov and Fang (1996a), we developed ideas that can be considered an extension of Torres-Verdin and Habashy's (1994) method. Expression (2) can be rewritten in operator form:

$$\mathbf{E}^a = \mathbf{C}[\mathbf{E}^a], \tag{8}$$

where $\mathbf{C}[\mathbf{E}^a]$ is an integral operator on the anomalous field $\mathbf{E}^a$:

$$\mathbf{C}[\mathbf{E}^a] = \mathbf{A}[\mathbf{E}^n] + \mathbf{A}[\mathbf{E}^a], \tag{9}$$

and $\mathbf{A}$ is a linear scattering operator:

$$\mathbf{A}[\mathbf{E}] = \iiint_D \underset{\sim}{\mathbf{G}}^n(\mathbf{r}_j \mid \mathbf{r})\Delta\tilde{\sigma}(\mathbf{r})\mathbf{E}(\mathbf{r})\,dv. \tag{10}$$

Zhdanov and Fang (1996a) analyze different methods of determining an optimal $\underset{\sim}{\lambda}$. They show that one can use the following condition to determine $\underset{\sim}{\lambda}$:

$$\left\| \underset{\sim}{\lambda}(\mathbf{r}_j)\mathbf{E}^n(\mathbf{r}_j) - \iiint_D \underset{\sim}{\mathbf{G}}^n(\mathbf{r}_j \mid \mathbf{r})\Delta\tilde{\sigma}(\mathbf{r})[(\underset{\sim}{\mathbf{I}} + \underset{\sim}{\lambda})\mathbf{E}^n(\mathbf{r})]\,dv \right\| = \varphi(\underset{\sim}{\lambda}) = \min! \quad (19)$$

In numerical calculations we usually asume that $\underset{\sim}{\lambda}(\mathbf{r})$ is a slowly varying (tensor) function inside the anomalous domain D (the simplest form is a constant). Equation (19) then can be treated as an overdetermined problem and solved numerically by a least-squares method (Zhdanov and Fang, 1996a). After the $\underset{\sim}{\lambda}$ is found, the QL approximation to the field is calculated using

$$\mathbf{F}^a \approx \iiint_D \underset{\sim}{\mathbf{G}}^F(\mathbf{r}_j \mid \mathbf{r})\Delta\tilde{\sigma}(\mathbf{r})[\underset{\sim}{\mathbf{I}} + \underset{\sim}{\lambda}(\mathbf{r})]\mathbf{E}^n(\mathbf{r})\,dv. \quad (20)$$

where $\mathbf{F}^a$ stands for the anomalous electric ($\mathbf{E}^a$) or magnetic ($\mathbf{H}^a$) field observed outside the scatterer (e.g., at surface of the Earth), and $\underset{\sim}{\mathbf{G}}^F$ is the appropriate (electric or magnetic) Green's function.

2.3 Comparison

In their roles relating unknown anomalous or total fields to the incident field, the electrical reflectivity tensor $\underset{\sim}{\lambda}$ of the QL approximation and the scattering tensor $\underset{\sim}{\Gamma}$ of the extended Born approximation are themselves related by the simple formula:

$$\underset{\sim}{\lambda} = \underset{\sim}{\Gamma} - \underset{\sim}{\mathbf{I}}. \quad (21)$$

The two approximations differ significantly, however, in computing these tensors. The scattering tensor $\underset{\sim}{\Gamma}$ is defined explicitly by expression (7). The accuracy of the extended Born approximation depends on how well the integral in Eq. (5) is approximated by taking the constant value for the field $\mathbf{E}(\mathbf{r}_j)$. Because the Green's dyadic is strongly peaked for values $\mathbf{r} \approx \mathbf{r}_j$, the approximation should be good if the field itself is not varying rapidly at $\mathbf{r}_j$. Habashy et al. (1993) called this the "localized approximation."

The QL approximation determines the electrical reflectivity tensor by solving a minimization problem (Eq. 19) on a coarse grid. The accuracy of QL approximation depends only on the accuracy of this discretization of $\underset{\sim}{\lambda}$ and, in principle, can be made arbitrarily good, though care may be needed with a fine discretization, because Eq. (19) can become underdetermined.

3 Numerical examples of the QL approximation

This section compares the fields obtained by solving the integral equation (2) numerically, by computing the Born approximation (3), and by computing the QL approximation (15). Figure 1 shows the 3-D geoelectrical model, which consists of a homogeneous half-space of resistivity 100 ohm-m and a conductive rectangular inclusion with resistivity 1 ohm-m. The EM field in the model is excited by a horizontal rectangular loop, which is 10 × 10 m, carries a current of 1 A, and is 50 m to the left of the model, We have used the full integral-equation (IE) code, SYSEM (Xiong, 1992), and QL code, SYSEMQL (Zhdanov and Fang, 1996a) for computing the frequency-domain response of the complex conductivity structure along profiles parallel to the x-axis.

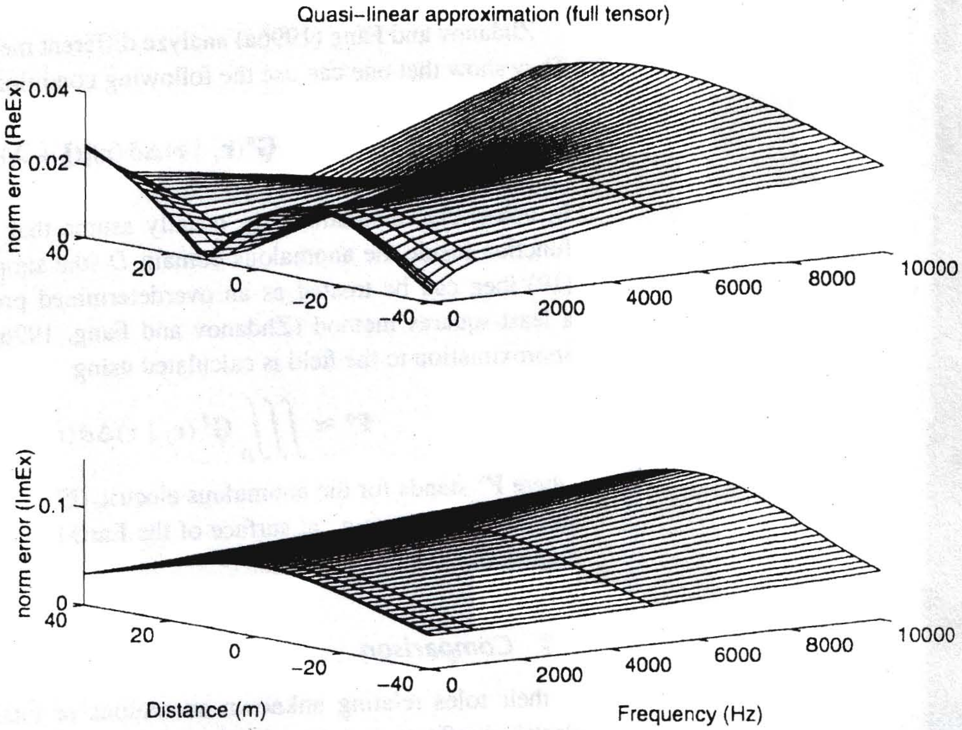

Figure 2. Numerical comparison of full IE solution and QL approximation computed for Model 1 (Fig. 1) at the frequency range from 0.1 Hz to 10 kHz. Calculations were performed for the receivers located along profiles parallel to the y-axis on the surface. Plots show the differences between IE solution and QL approximation for x-component of the secondary electric field normalized by the value of corresponding component of the field at the point $y = 40$ (normalized error).

Figures 2 and 3 compare the different solutions for real and imaginary parts of the anomalous electrical field E_x^a for different frequencies. The point $x = 0$ along each profile corresponds to the location of the conductive rectangular inclusion center. Figure 2 shows the differences between IE solution and QL approximation, normalized by the value of the corresponding component of the field at the point $y = 40$. The accuracy of the QL approximation for the electric-field components is within 5% for frequencies from 0.1 Hz to 10 kHz. Figure 3 presents the differences between the IE solution and Born approximation, normalized by the value of the corresponding component of the field at the point $y = 40$. The QL approximation produces a reasonable result, whereas the conventional Born approximation is far off the mark.

The next set of comparisons uses the same geometric model, but varies the body's conductivity. We selected four different resistivities of the inclusion: 1 ohm-m, 0.1 ohm-m, 0.01 ohm-m, and 0.001 ohm-m. Figure 4 shows the differences between the IE solution and the QL approximation, at a frequency 0.1 Hz, normalized by the value of the corresponding component of the field at the point $y = 40$. One of the horizontal axes on Fig. 4 is the resistivity contrast $C = \rho_i/\rho_b$, where $\rho_b = 100$ ohm-m is the resistivity of the background, and ρ_i is the resistivity of the conductive inclusion. The errors of QL approximation are generally small and grow only for very-high-conductivity contrasts, equal to $1/C = 10^5$, reaching about 10% in extremum point for the electric field. For lower-conductivity contrasts, the relative errors are below 5%.

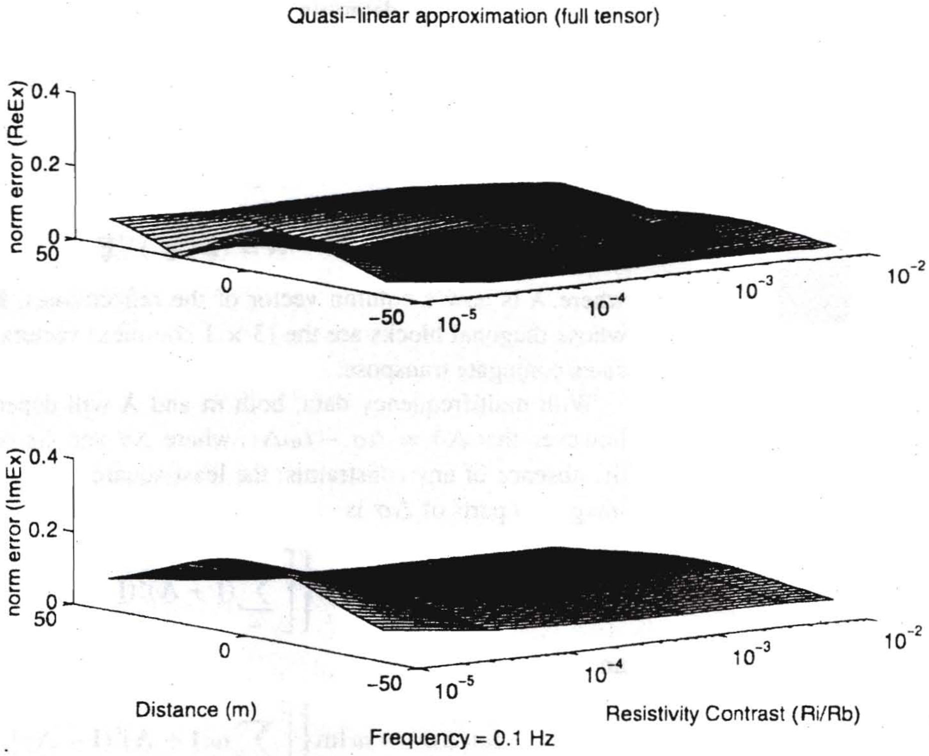

Figure 4. Numerical comparison of full IE solution and QL approximation computed for Model 1 (Fig. 1) at the resistivity ratio of inclusive body to the background range from 0.00001 to 0.01 (or -5 to -2 in log scale). Calculations were performed for the receivers located along profiles parallel to the y-axis on the surface. Plots show the differences between IE solution and QL approximation for x-component of the secondary electric field at the frequency 0.1 Hz normalized by the value of corresponding component of the field at the point $y = 40$ (normalized error).

which is linear with respect to $\underset{\sim}{\mathbf{m}}(\mathbf{r})$ (the original Eq. 20 is nonlinear with respect to $\Delta\tilde{\sigma}$ because the reflectivity tensor depends implicity on $\Delta\tilde{\sigma}$). It has the same structure as the Born approximation for the anomalous field, with the modified material property tensor $\underset{\sim}{\mathbf{m}}(\mathbf{r})$ replacing the anomalous conductivity $\Delta\tilde{\sigma}(\mathbf{r})$. We call Eq. (23) a *quasi-Born approximation*, and its solution (for $\underset{\sim}{\mathbf{m}}$), a *quasi-Born inversion.*

The reflectivity tensor $\underset{\sim}{\boldsymbol{\lambda}}$ can be computed from $\underset{\sim}{\mathbf{m}}$, because

$$\mathbf{E}^a(\mathbf{r}_j) \approx \iiint_D \underset{\sim}{\mathbf{G}}^E(\mathbf{r}_j \mid \mathbf{r})\underset{\sim}{\mathbf{m}}(\mathbf{r})\mathbf{E}^n(\mathbf{r})\,dv \approx \underset{\sim}{\boldsymbol{\lambda}}(\mathbf{r}_j)\mathbf{E}^n(\mathbf{r}_j). \tag{24}$$

Once $\underset{\sim}{\mathbf{m}}$ and $\underset{\sim}{\boldsymbol{\lambda}}$ are known, the anomalous conductivity $\Delta\tilde{\sigma}$ follows from Eq. (22). This inversion scheme reduces the original nonlinear inverse problem to three linear steps:

- inversion of the quasi-Born equation (23) for $\underset{\sim}{\mathbf{m}}$;
- computation of the integral (24) to obtain $\underset{\sim}{\boldsymbol{\lambda}}$; and
- (local) inversion of Eq. (22) to obtain the conductivity $\Delta\tilde{\sigma}$.

We call this procedure a *QL inversion.* As we explain further below, these three steps *do not* solve the full nonlinear inverse problem for $\Delta\tilde{\sigma}$ (mainly because the inversion in the first step is intrinsically nonunique), but they do provide the basis for an effective iterative solution. This iterative scheme resembles the source-type IE method of Habashy et al. (1994) and the modified gradient method of Kleinman and van den Berg (1993).

Equation (26) is overdetermined and can be inverted directly (in least-squares sense) by

$$\lambda_k = [\mathbf{E}^{n*}(\mathbf{r}_j)\cdot\mathbf{E}^n(\mathbf{r}_j)]^{-1}\mathbf{E}^{n*}(\mathbf{r}_j)\cdot\sum_{\ell=1,N}\iiint_{D_\ell}\underset{\sim}{\mathbf{G}}^E(\mathbf{r}_j \mid \mathbf{r})m_\ell\mathbf{E}^n(\mathbf{r})\,dv, \quad \mathbf{r}_j \in D_k, \tag{31}$$

or, in matrix form,

$$\boldsymbol{\lambda} = (\underset{\sim}{\mathbf{E}}^{n*}\underset{\sim}{\mathbf{E}}^n)^{-1}\underset{\sim}{\mathbf{E}}^{n*}\underset{\sim}{\mathbf{G}}^E\mathbf{m}, \tag{32}$$

where $\boldsymbol{\lambda}$ is now a column vector of the reflectivities; $\underset{\sim}{\mathbf{E}}^n$ is a block diagonal matrix whose diagonal blocks are the (3×1 complex) vectors $\mathbf{E}^n(\mathbf{r}_j)$; and the asterisk indicates conjugate transpose.

With multifrequency data, both $\mathbf{m}$ and $\boldsymbol{\lambda}$ will depend on frequency. We assume, however, that $\Delta\tilde{\sigma} = \Delta\sigma - i\omega\Delta\varepsilon$, where $\Delta\sigma$ and $\Delta\varepsilon$ do not depend on frequency. In the absence of any constraints, the least-squares solution of Eq. (29) for the real and imaginary parts of $\Delta\boldsymbol{\sigma}$ is

$$\operatorname{Re}(\Delta\boldsymbol{\sigma}) = \operatorname{Re}\left\{\left[\sum_\omega(\underset{\sim}{\mathbf{I}}+\underset{\sim}{\boldsymbol{\Lambda}})^*(\underset{\sim}{\mathbf{I}}+\underset{\sim}{\boldsymbol{\Lambda}})\right]^{-1}\sum_\omega(\underset{\sim}{\mathbf{I}}+\underset{\sim}{\boldsymbol{\Lambda}})^*\mathbf{m}\right\}, \tag{33}$$

and

$$\operatorname{Im}(\Delta\boldsymbol{\sigma}) = \omega\operatorname{Im}\left\{\left[\sum_\omega\omega(\underset{\sim}{\mathbf{I}}+\underset{\sim}{\boldsymbol{\Lambda}})^*(\underset{\sim}{\mathbf{I}}+\underset{\sim}{\boldsymbol{\Lambda}})\right]^{-1}\sum_\omega(\underset{\sim}{\mathbf{I}}+\underset{\sim}{\boldsymbol{\Lambda}})^*\mathbf{m}\right\}. \tag{34}$$

4.2 Regularized QL inversion

QL inversion requires the solution of Eq. (28) for $\mathbf{m}$, computation of λ_k by Eq. (31), and solution of Eq. (29) for $\Delta\tilde{\sigma}_j$. To obtain a stable, regularized solution, we introduce the functional

$$P^\alpha(\mathbf{m}) = \phi(\mathbf{m}) + \alpha S(\mathbf{m}), \tag{35}$$

where the misfit functional is specified as

$$\begin{aligned}\phi(\mathbf{m}) &= \|\underset{\sim}{\mathbf{G}}^F\mathbf{m}-\mathbf{F}\|^2 + \|\mathbf{m}-(\underset{\sim}{\mathbf{I}}+\underset{\sim}{\boldsymbol{\Lambda}})\Delta\boldsymbol{\sigma}\|^2\\ &= (\underset{\sim}{\mathbf{G}}^F\mathbf{m}-\mathbf{F})^*(\underset{\sim}{\mathbf{G}}^F\mathbf{m}-\mathbf{F}) + [\mathbf{m}-(\underset{\sim}{\mathbf{I}}+\underset{\sim}{\boldsymbol{\Lambda}})\Delta\boldsymbol{\sigma}]^*[\mathbf{m}-(\underset{\sim}{\mathbf{I}}+\underset{\sim}{\boldsymbol{\Lambda}})\Delta\boldsymbol{\sigma}].\end{aligned} \tag{36}$$

The misfit functional tracks the solution of both equations (28) and (29). The stabilizer is

$$S(\mathbf{m}) = \|\mathbf{m}-\mathbf{m}_p\|^2 = (\mathbf{m}-\mathbf{m}_p)^*(\mathbf{m}-\mathbf{m}_p). \tag{37}$$

The prior model $\mathbf{m}_p$ is some reference model, selected on the basis of all available geological and geophysical information about the area under investigation. The scalar multiplier α is a regularization parameter.

The misfit functional provides the solution that best fits the observed data $\mathbf{F}$, whereas the stabilizing functional ties the solution to the prior model $\mathbf{m}_p$. The regularization parameter α controls the trade-off between these two goals. Principles for determining the regularization parameter α are discussed by Tikhonov and Arsenin (1977) and Zhdanov and Keller (1994). We use a simple numerical method to determine the parameter α. Consider the progression of numbers

$$\alpha_k = \alpha_0 q^k; \quad k = 0, 1, 2, \ldots, n; \quad q > 0. \tag{38}$$

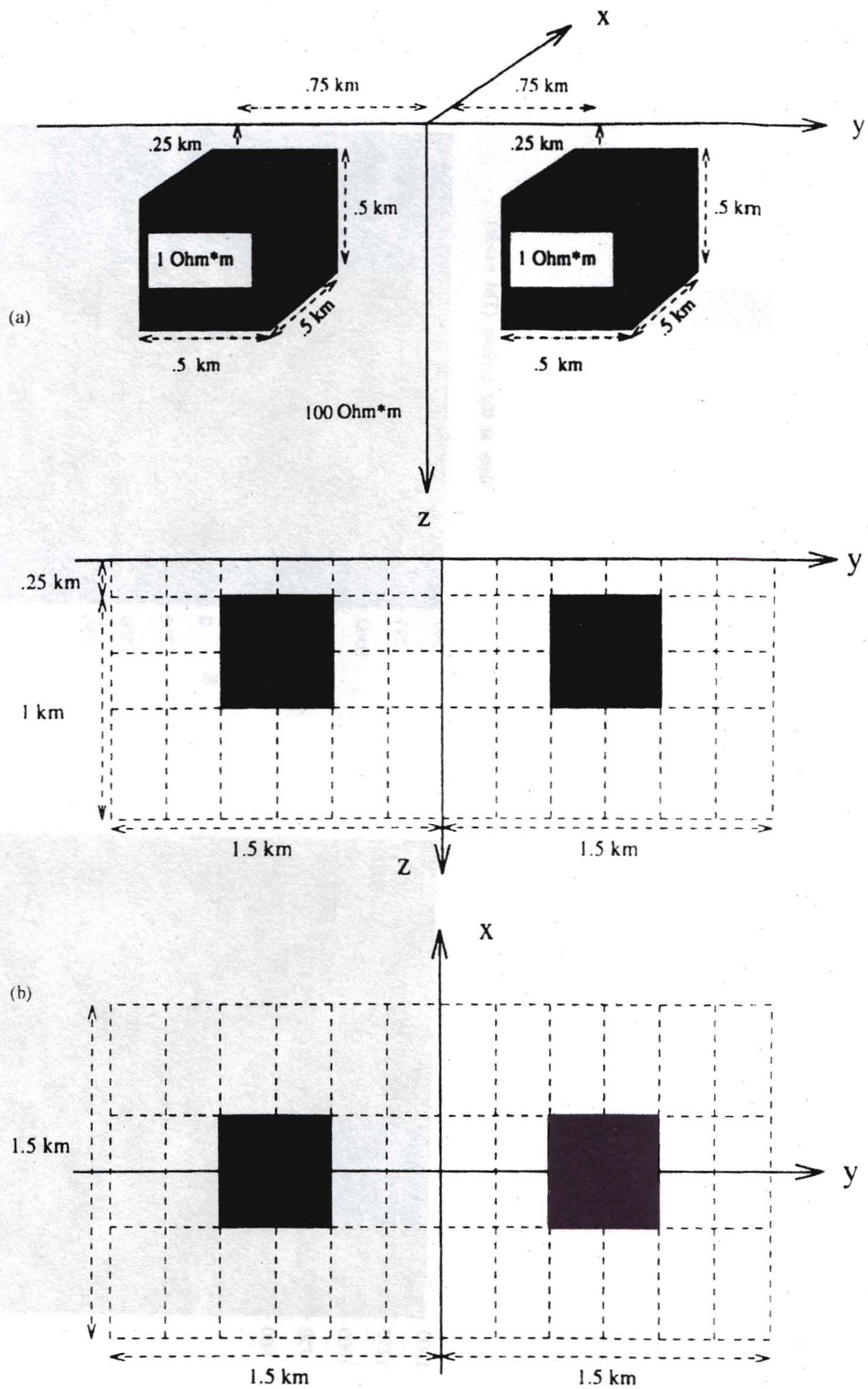

Figure 5. (a) Three-dimensional model of two rectangular conductive structures in a homogeneous half-space, excited by a plane wave (Model 2); (b) division of model into substructures used for inversion.

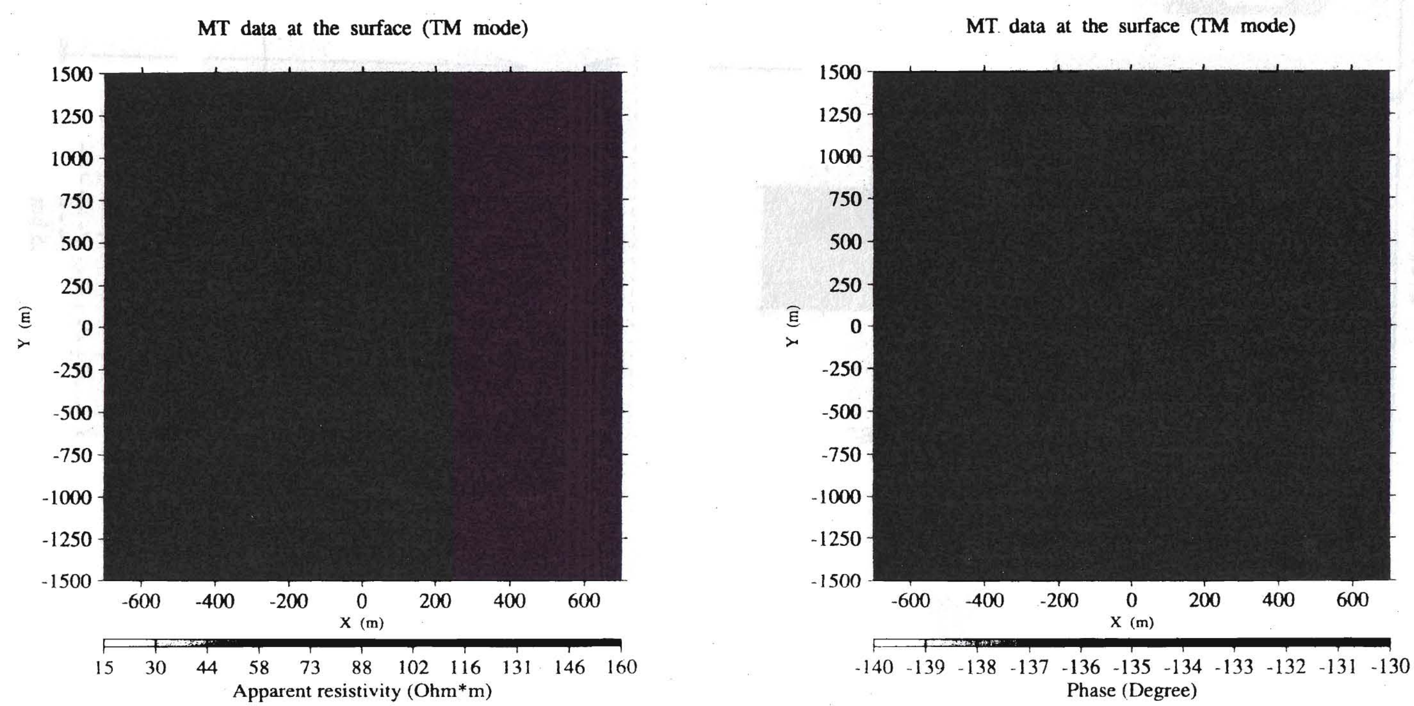

Figure 1. (a) Apparent resistivity amplitude distribution for the model shown in Fig. 5, calculated on the surface of the Earth for a frequency of 1 Hz. (b) Impedance phase distribution for the model shown in Fig. 5, calculated for a frequency of 1 Hz.

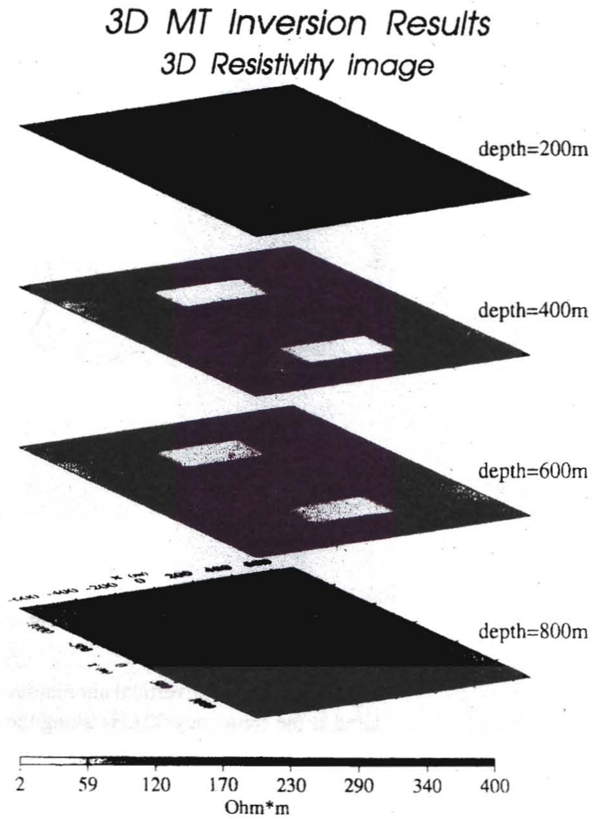

Figure 10. The volume image of the inverted model computed from EM data (with 5% noise added) collected along 15 profiles on the surface of the Earth for four frequencies (10, 1, 0.5, and 0.2 Hz) for the model shown in Fig. 5.

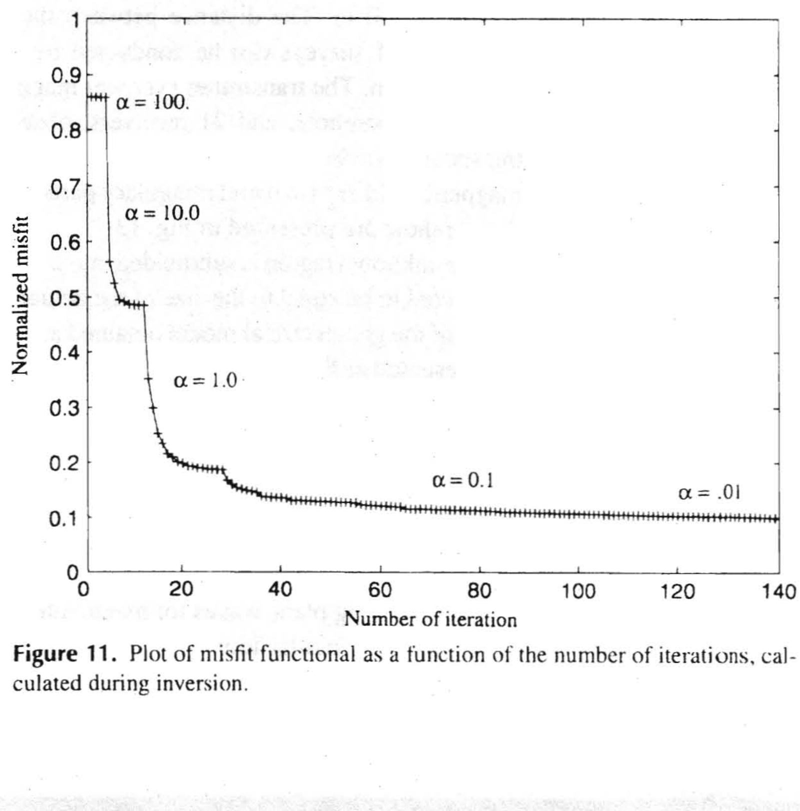

Figure 11. Plot of misfit functional as a function of the number of iterations, calculated during inversion.

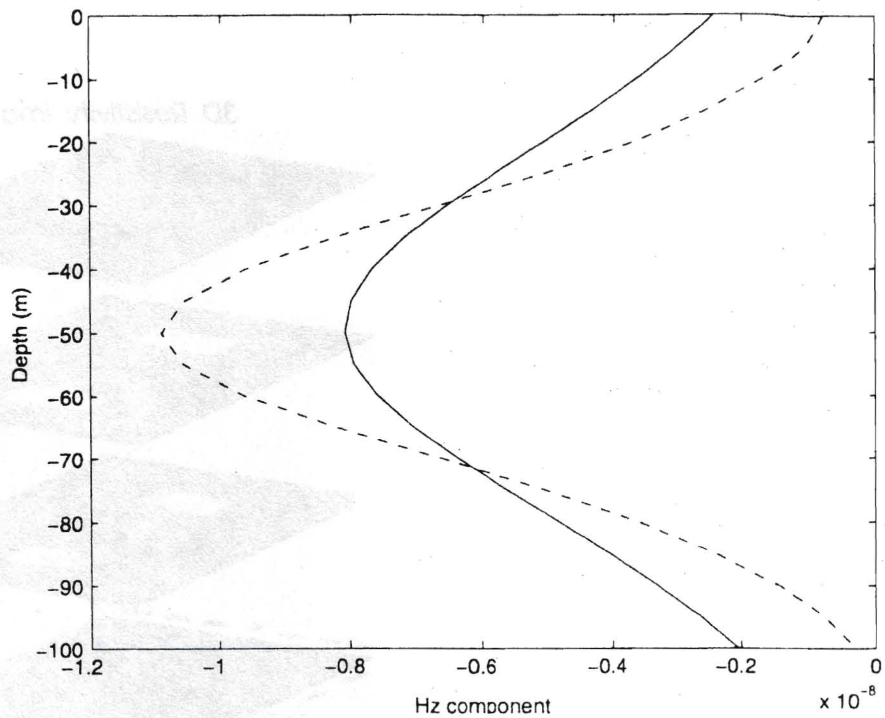

Figure 13. Plots of vertical anomalous magnetic field H_z^a (real and imaginary parts) calculated at the frequency 50 kHz along the borehole.

5.2 *Cross-borehole vertical magnetic dipole excitation model*

Let us consider a model simulating an orebody (Bertrand and McGaughey, 1994). We present the orebody as a cube with side 20 m and resistivity 1 ohm-m embedded in a homogeneous media with resistivity 100 ohm-m. This model simulates typical massive-sulfide deposits. The orebody is located exactly in the middle of the two boreholes at a depth of 40 m. The distance between the boreholes is 100 m (Fig. 12a). Cross-borehole EM surveys can be conducted by the frequency-domain vertical magnetic dipole system. The transmitter (vertical magnetic dipole) is located at a depth of 50 m in the first borehole, and 21 receivers, observing the vertical magnetic field, are in the second borehole, from a depth of 0 to 100 m. The plots of the vertical anomalous magnetic field H_z^a (real and imaginary parts) calculated for the frequency 50 kHz along the borehole are presented in Fig. 13.

The unknown region is subdivided into 27 substructures: The size of the substructures is selected to be equal to the size of the actual conducting body (Fig. 12b). The vertical slices of the geoelectrical model obtained as the result of the inversion for borehole data are presented at Fig. 14. Comparison of these results with the original model (Fig. 12a) shows that QL inversion produces a reasonable model of the target.

6 Conclusion

We have developed a fast algorithm for 3-D EM inversion based on the QL approximation of forward modeling. The method works for models with various sources of excitation, including plane waves for magnetotellurics, horizontal bipoles, vertical bipoles, horizontal rectangular loops, vertical magnetic dipoles, and the loop-loop system for surface (and airborne) electromagnetics.

References

Born, M., 1933, *Optics*: Springer Pub. Co., Inc.

Berdichevsky, M. N., and Zhdanov, M. S., 1984, Advanced theory of deep geomagnetic sounding: Elsevier Science Publ. Co., Inc.

Bertrand, M. J., and McGaughey, J., 1994, Crosshole EM detectability of high-conductivity contrast anomalies: 64th Ann. Mt., Soc. Expl. Geophys. Expanded Abstracts, 407–410.

Druskin, V., and Knizhnerman, L., 1994, Spectral approach to solving three-dimensional Maxwell's diffusion equations in the time and frequency domains: Radio Sci., **29**, 937–953.

Eaton, P. A., 1989, 3-D electromagnetic inversion using integral equations: Geophys. Prosp., **37**, 407–426.

Gusarov, A. L., 1981, About the uniqueness of the solution of the magnetotelluric inverse problem, *in* Mathematical models in geophysical problems: Moscow Univ. Press, 31–80.

Habashy, T. M., Groom, R. W., and Spies, B. R., 1993, Beyond the Born and Rytov approximations: A nonlinear approach to EM scattering: J. Geophys. Res., **98**, 1759–1775.

Habashy, T. M., Oristaglio, M. L., and de Hoop, A. T., 1994, Simultaneous nonlinear reconstruction of two-dimensional permittivity and conductivity: Radio Sci., **29**, 1101–1118.

Hohmann., G. W., 1975, Three-dimensional induced polarization and EM modeling: Geophysics, **40**, 309–324.

Kleinman, R. E., and van den Berg, P. M., 1993, An extended range-modified gradient technique for profile inversion: Radio Sci., **28**, 877–884.

Madden, T. R., and Mackie, R. L., 1989, Three-dimensional magnetotelluric modeling and inversion: Proc. IEEE, **77**, 318–332.

Newman, G. A., and Alumbaugh, D. L., 1995, 3-D massively parallel electromagnetic inversion: PIERS Proc., Univ. of Washington, 324.

Smith, J .T., and Booker, J. R., 1991, Rapid inversion of two- and three-dimensional magnetotelluric data: J. Geophys. Res., **96**, 3905–3922.

Svetov, B. S., and Gubatenko, V. P., 1985, About the equivalence of the system of the extraneous electric and magnetic currents: Radiotechniques and electronics, No. 4, 31–40.

Tikhonov, A. N., and Arsenin, V. Y., 1977, Solution of ill-posed problems: W. H. Winston and Sons.

Torres-Verdín, C., and Habashy, T. M., 1994, Rapid 2.5-dimensional forward modeling and inversion via a new nonlinear scattering approximation: Radio Sci., **29**, 1051–1079.

———1995a, Two-steps linear inversion: Radio Sci., **29**, 1051–1079.

———1995b, An overview of the extended Born approximation as a nonlinear scattering approach, and its application to cross-well resistivity imaging: PIERS Proc., Univ. of Washington, 321.

Tripp, A. C., 1990, Group theoretic reduction of the EM impedance matrix for large-contrast symmetric prisms in a layered earth: Pageoph, **133**, 127–147.

Tripp, A. C., and Hohmann, G. W., 1993, Three-dimensional EM cross-well inversion: IEEE Trans. Geosci. Remote Sensing, **31**, 121–126.

The reflectivity $\boldsymbol{\lambda}_N$ is determined from m_N using Eq. (31):

$$\underset{\sim}{\mathbf{E}}^n \boldsymbol{\lambda}_N = \mathbf{G}^E \mathbf{m}_N, \tag{A5}$$

Note that the anomalous conductivity has to satisfy the condition (componentwise)

$$\mathrm{Re}(\Delta\tilde{\boldsymbol{\sigma}}_{N-1}) \geq -\sigma_n; \quad \mathrm{Im}(\Delta\boldsymbol{\sigma}_{N-1}) \leq \omega\varepsilon_n \tag{A6}$$

because the electrical conductivity and dielectric permittivity have to be positive. Therefore, the conductivity $\Delta\tilde{\boldsymbol{\sigma}}_{N-1}$ can be found by using Eqs. (33) and (A6) with the following conditions (componentwise):

$$\mathrm{Re}(\Delta\tilde{\sigma}_{N-1}) = \mathrm{Re}\left[\sum_\omega [(1+\lambda_{N-1})^*(1+\lambda_{N-1})]\right]^{-1}\left[\sum_\omega (1+\lambda_{N-1})^* m_{N-1}\right]$$
$$= a_{N-1} \quad \text{for } a_{N-1} \geq -\sigma_n \tag{A7}$$

and

$$\mathrm{Re}(\Delta\tilde{\sigma}_{N-1}) = -\tfrac{1}{2}\sigma_n, \quad \text{for } \mathbf{a}_{N-1} \leq -\sigma_n. \tag{A8}$$

Similarly,

$$\mathrm{Im}(\Delta\tilde{\sigma}_{N-1}) = -\omega\,\mathrm{Im}\left\{\left[\sum_\omega \omega(1+\lambda_{N-1})^*(1+\lambda_{N-1})\right]^{-1}\right.$$
$$\left.\times\left[\sum_\omega (1+\lambda_{N-1})^* m_{N-1}\right]\right\} = b_{N-1},$$

$$\text{for } b_{N-1} < \omega\varepsilon_n$$
$$\mathrm{Im}(\Delta\tilde{\sigma}_{N-1}) = \tfrac{1}{2}\omega\varepsilon_n, \quad \text{for } b_{N-1} \geq \omega\varepsilon_n.$$

The initial iteration should be done using the formula

$$\mathbf{m}_1^\alpha = \mathbf{m}_0^\alpha + \delta\mathbf{m}_0 = \mathbf{m}_0^\alpha - k_0^\alpha\,[\underset{\sim}{\mathbf{G}}^{F*}(\underset{\sim}{\mathbf{G}}^F \mathbf{m}_p - \mathbf{F})], \tag{A9}$$

where

$$\mathbf{m}_p = (\underset{\sim}{\mathbf{I}} + \underset{\sim}{\boldsymbol{\Lambda}}_p)\Delta\boldsymbol{\sigma}_p$$

The second iteration is

$$\mathbf{m}_2^\alpha = \mathbf{m}_1^\alpha + \boldsymbol{\delta}\mathbf{m}_1 = \mathbf{m}_1^\alpha - k_1^\alpha\,\ell^\alpha(\mathbf{m}_1), \tag{A10}$$

where

$$\ell^\alpha(\mathbf{m}_1) = \mathbf{G}^{F*}(\underset{\sim}{\mathbf{G}}^F \mathbf{m}_1 - \mathbf{F}) + [\mathbf{m}_1 - (\underset{\sim}{\mathbf{I}} + \underset{\sim}{\boldsymbol{\Lambda}}_1)\Delta\boldsymbol{\sigma}_p] + \alpha\,(\mathbf{m}_1 - \mathbf{m}_p). \tag{A11}$$

The coefficient k_n^α can be determined from the condition

$$P^\alpha\left(\mathbf{m}_{N+1}^\alpha\right) = P^\alpha\left[\mathbf{m}_N^\alpha - k_N^\alpha\,\ell^\alpha(\mathbf{m}_N)\right] = f\left(k_N^\alpha\right) = \min!$$

Solution of this minimization problem gives the following best estimation for the length of the step:

$$k_N^\alpha = \frac{\ell^{\alpha*}(\mathbf{m}_N^\alpha)\ell^\alpha(\mathbf{m}_N^\alpha)}{\ell^{\alpha*}(\mathbf{m}_N^\alpha)(\mathbf{G}^{F*}\mathbf{G}^F + \alpha\underset{\sim}{\mathbf{I}})\ell^\alpha(\mathbf{m}_N^\alpha)}. \tag{A12}$$

Using Eqs. (A2), (A3), and (A12), we can obtain $\mathbf{m}$ iteratively.